

Astrophysical ZeV acceleration in the relativistic jet from an accreting supermassive blackhole

Toshikazu Ebisuzaki¹ and Toshiki Tajima²

`ebisu@postman.riken.jp`

Received _____; accepted _____

to be submitted to *Astrophysical Journal*

¹RIKEN, Wako, Saitama, Japan

²University of California, Irvine, CA, 92679

ABSTRACT

An accreting supermassive blackhole, the central engine of active galactic nucleus (AGN), is capable of exciting extreme amplitude Alfvén waves whose wavelength (wave packet) size is characterized by its clumpiness. The ponderomotive force and wakefield are driven by these Alfvén waves propagating in the AGN (blazar) jet and accelerate protons/nuclei to extreme energies beyond Zetta-electron volt ($\text{ZeV} = 10^{21}$ eV). Such acceleration is prompt, localized, and does not suffer from the multiple scattering/bending enveloped in the Fermi acceleration that causes excessive synchrotron radiation loss beyond 10^{19} eV. The production rate of ZeV cosmic rays is found to be consistent with the observed gamma-ray luminosity function of blazars and their time variabilities.

Subject headings: acceleration of particles — accretion, accretion disks — relativistic processes — galaxies: jets — galaxies: nuclei — gamma rays: galaxies

1. Introduction

The origin of ultra-high energy cosmic rays (UHECRs) with energies 10^{20} eV remains a puzzle of astrophysics. It is generally believed to be extragalactic (Kotera & Olinto (2011), references therein). The production of UHECRs has been discussed mainly in the framework of the Fermi acceleration, in which charged particles gain energy through a numerous number of scatterings by the magnetic clouds. One of the necessary conditions of Fermi acceleration is the magnetic confinement: the Hillas criterion sets a constraint on the product of the magnetic field strength B and extension R of the candidate objects (Hillas criterion; Hillas (1984)): $W \leq W_{\max} \sim z(B/1\mu\text{G})(R/1\text{kpc}) \text{ EeV}$, where z is the charge of the particle. The possible candidate objects (but only marginally satisfy the Hillas criterion for 10^{20} eV) are neutron stars, active galactic nuclei (AGN), gamma-ray bursts (GRBs), and accretion shocks in the intergalactic space. However, the acceleration of 10^{20} eV particles even in those candidate objects is not easy for the Fermi mechanism because of 1) a large number of scatterings necessary to reach highest energies, 2) energy losses through the synchrotron emission at the bending associated with scatterings, and 3) difficulty in the escape of particles which are once magnetically confined in the acceleration domain (Kotera & Olinto (2011)).

Tajima & Dawson (1979) first pointed out that intense electromagnetic fields create the plasma wakefield in which charged particles are accelerated by the Lorentz invariant ponderomotive force in the longitudinal direction over a long distance. The wakefield acceleration has advantages over the Fermi mechanism in producing UHECRs for the following reasons:

1. The plasma wakefield provides an extremely high accelerating field.
2. It does not require particle bending, which would cause severe synchrotron radiation

losses in extreme energies.

3. The wakefield and particles move in the collinear direction at the same velocity, the speed of light, so that the acceleration has a built-in coherence, while the Fermi acceleration mechanism, based on multiple scatterings, is intrinsically incoherent and stochastic.
4. No escape problem exists. Particles can escape from the acceleration region since the wakefield naturally decays out.
5. Whenever and wherever intense electromagnetic waves (with sufficiently high frequencies) are excited, such waves tend to exhibit coherent dynamics (see later for details).

In fact the “**wakefield accelerator**” concept is believed to be a promising candidate for a future-generation artificial accelerator (e.g. Leemans et al. (2011)). It has been under intensive research (Esarey et al. (2009)).

Takahashi et al. (2000) and Chen et al. (2002) demonstrated that intense Alfvén waves produced by a collision of neutron stars can create wakefields to accelerate charged particles beyond 10^{20} eV. Although such a neutron star collision is believed to be related to short gamma-ray bursts (Nakar (2007)), it is rather rare for two neutron stars to hit each other directly: It requires the same masses, otherwise the tidal field of the more massive star destroys the less massive one to form accretion disk. Chang et al. (2009) conducted one-dimensional numerical simulation showing that whistler waves emitted from an AGN produce wakefields to accelerate UHECR.

The accreting supermassive blackhole, the central engine of an AGN, is one of the candidates for wakefield acceleration. The accretion disk repeats transitions between highly magnetized (low-beta) state and weakly magnetized (high-beta) state (Shibata et

al. (1990)). In fact, O'Neill et al. (2011) have found that magnetic transitions with 10-20 orbital periods are predominant in the inner disk through their 3D simulation. Strong pulses of Alfvén waves excited in the accretion disk at the transition can create intense wakefields in the relativistic jet launched from the innermost region of the accretion disk. Our analysis finds that these wakefields are natural to accelerate protons and nuclei up to extreme energies of ZeV (10^{21} eV).

In the present paper we carry out a quantitative evaluation of the system of an accreting blackhole which consists of a blackhole itself, an accretion disk, and relativistic jets (figure 1), to lead to the generation of UHECRs beyond 10^{20} eV. The paper is organized as follows. We introduce our model for the intense wakefield generation that is not hampered by the Fermi mechanism limitations in Sec. 2 and find that the highest energy is achievable around an accreting blackhole (AGN) in Sec. 3. Astrophysical implications are discussed in Sec. 4.

2. Intense wakefield mechanism

An accretion disk is formed around a blackhole when gas accretes onto it. Since the angular velocity is higher in inner orbits, there arises a strong shear flow between gases circulating at different radii in the disk. Since the gas is almost fully ionized and Ohmic loss is negligible, magnetic fields are stretched and amplified by the shear motion. The resultant toroidal magnetic field acts as an enhanced friction between gases circulating in the different orbits and transfers the angular momentum outward, while gas is pushed inward because of the reaction of the momentum exchange.

The inner edge of the accretion disk is located around $R = 3R_g$, where

$$R_g = 2GM/c^2 = 3.0 \times 10^{13}(m/10^8) \text{ cm} \quad (1)$$

is the gravitational radius of the blackhole. Here, m is the mass of the blackhole in the unit

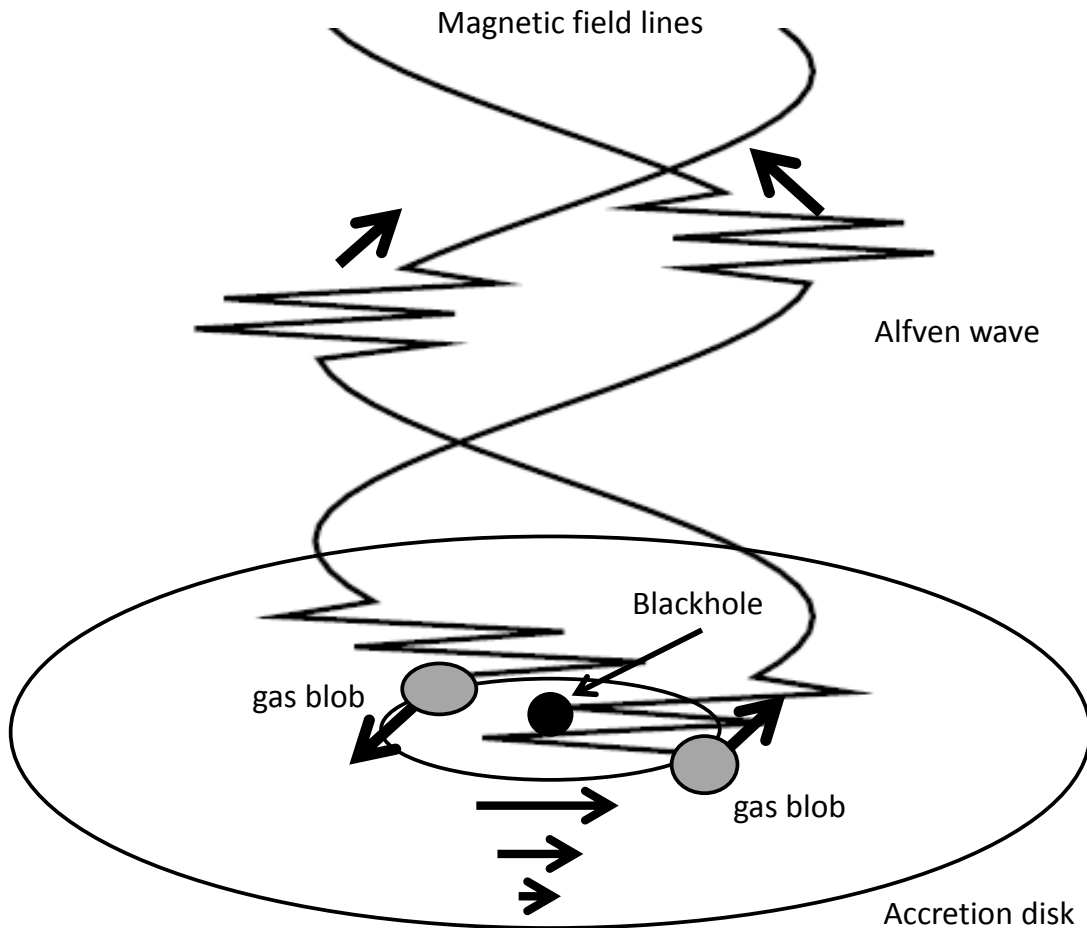


Fig. 1.— Schematic diagram of the production of intensive Alfven waves in an accretion disk. A gas blob formed near the inner edge of the accretion disk severely shakes the magnetic fields and excites relativistic Alfven waves, which propagate along the magnetic field line of the jet.

of solar mass (2.0×10^{33} g). An ergo-sphere appears just outside of causality horizon of the blackhole. The gas inside the ergo-sphere and the outside the horizon can extract the rotational energy from the blackhole, if they are magnetized. They drive relativistic jets in the two axial directions of the accretion disk (Blandford & Znajek (1977)). The Lorentz factor Γ of the bulk motion of the jet is observed as $10 \sim 30$ in the case of active galactic nuclei.

According to Shibata et al. (1990), the accretion disk makes transition between two states: In the weakly magnetized state, magnetic fields are amplified by a strong shear flow, grow until at a certain point, and decay out, in other words, the disk makes transitions between these two states repeatedly. As a result, strong fluctuations are induced in the innermost region of the accretion region ($R < 10R_g$). The physical parameters in this innermost region ($R < 10R_g$) are estimated according to Shakura & Sunyaev (1973):

$$\varepsilon_D = 6.6 \times 10^6 \quad (m/10^8)^{-1} \quad \text{erg cm}^{-3}, \quad (2)$$

$$n_D = 2.9 \times 10^{14} \quad (\dot{m}/0.1)^{-2} (m/10^8)^{-1} \quad \text{cm}^{-3}, \quad (3)$$

$$Z_D = 2.2 \times 10^{13} \quad (\dot{m}/0.1)(m/10^8) \quad \text{cm}, \quad (4)$$

$$B_D = 1.8 \times 10^3 \quad (m/10^8)^{-1/2} \quad \text{G}, \quad (5)$$

where \dot{m} is the accretion rate normalized to the critical accretion rate ($\dot{M}_c = L_{\text{Edd}}/0.06c^2$; Shakura & Sunyaev (1973)). The viscosity parameter α is assumed to be 0.1 in the present paper. From the definition of m and \dot{m} , the total luminosity of the accreting blackhole is given by

$$L_{\text{tot}} = 1.3 \times 10^{45} (\dot{m}/0.1)(m/10^8) \quad \text{erg s}^{-1}. \quad (6)$$

The wavelength λ_A of Alfvén waves emitted from the accretion disk is calculated as (Matsumoto & Tajima (1995)):

$$\lambda_A = (V_{\text{AD}}/C_{\text{sD}})(\Omega/A)Z_D = 4B_D Z_D / 3(4\pi\varepsilon_D)^{1/2} = 5.8 \times 10^{12} (\dot{m}/0.1)(m/10^8) \quad \text{cm}, \quad (7)$$

where V_A is the Alfvén velocity in the accretion disk, which is calculated as:

$$V_{AD} = B_D / \sqrt{4\pi m_H n_D} = 2.4 \times 10^7 (\dot{m}/0.1), \quad (8)$$

and C_{sD} is the sound velocity in the accretion disk:

$$C_{sD} = \sqrt{\varepsilon_D / m_H n_{SS}}, \quad (9)$$

where m_H is the proton mass. We assume magnetic field in the accretion disk as B_{SS} and the Keplerian rotation of gas inside the disk, i.e. $\Omega/A = 4/3$. The magnetic energy E_B stored in the innermost region of the accretion disk ($R < 10R_g$) is estimated as:

$$E_B = (B_D^2 / 4\pi) \pi (10R_g)^2 Z_D = 1.6 \times 10^{48} (\dot{m}/0.1) (m/10^8)^2 \text{ erg.} \quad (10)$$

The Alfvén waves excited in the accretion disk propagate along the global magnetic field of the jet. The normalized vector potential a is the Lorentz-invariant strength parameter of the wave (Esarey et al. (2009)) just above the disk is calculated as:

$$a_0 = eE / m_e \omega_{AC} = 2.3 \times 10^{10} (\dot{m}/0.1)^{3/2} (m/10^8)^{1/2}, \quad (11)$$

where we used $E = (V_{AD}/c)^{1/2} B_D$ and $\omega_A = 2\pi V_{AJ}/\lambda_A \simeq 2\pi c/\lambda_A$. The former is came of the conservation of Alfvén energy flux, i.e., $\Phi_{AJ} (= cE \times B / 4\pi) = \Phi_{AD} (= V_{AD} B_D^2 / 4\pi)$. We find that a is much greater than unity for a large class of AGN disks and thus highly relativistic wakefield dynamics is anticipated (Ashour-Abdalla et al. (1981)), where the Alfvén flux inside of the jet assumed to be inversely proportional to πb^2 and b to the square root of the distance D : $b = 10R_g (D/3R_g)^{1/2}$. This scaling is consistent with the VLBI observation of the jet of M87, the closest AGN (Asada et al. (2012)). In such a case, a of the wave propagating in the jet is calculated as:

$$a = a_0 (D/3R_g)^{-1/2}, \quad (12)$$

where D is the distance from the black hole along the jet. The Lorentz factor γ of the quivering motion of particles in the wave is of the order of a , i.e., $\gamma \sim a$.

The kind of Alfvén waves that are anticipated in the AGN jets have an extremely large value of a . It is a challenge for us to explore the physics of extremely relativistic wave dynamics (it is even beyond what has been called the "ultrarelativistic regime" (Mourou et al. (2006)) and has been seldom considered. Ashour-Abdalla et al. (1981) have considered such a regime in which protons begin to behave similarly to positrons. Bulanov et al. (2013) have analysed some aspect of the ponderomotive acceleration. We shall take liberal indulgence into such works in the past as our guidance in extending them for the present purpose.

The Alfvén pulse generation, its collinear propagation feature, and its ponderomotive acceleration are all under coherent dynamics. In other words, the phase between the specific wave and particles to be accelerated are tightly locked because the phase velocity of these waves (including the Alfvén pulse in the jet under consideration) is very close to the speed of light. Further note that the wakefield in one dimension is robust because of the relativistic coherence (Tajima (2011)). The mechanism known as the dephasing (along with the pump depletion; Tajima & Dawson (1979); Esarey et al. (2009)) determines the maximum energy gain as well as the spectrum (Mima et al. (1991); Chen et al. (2002)).

We focus on the wave modes propagating parallel to the jet magnetic field, since these modes are effective for the linear acceleration to highest energies. The angular frequency of the Alfvén wave is:

$$\omega_A = 2\pi V_{AJ}/\lambda_A \cong 2\pi c/\lambda_A = 3.2 \times 10^{-2} (\dot{m}/0.1)^{-1} (m/10^8)^{-1} \text{ Hz}, \quad (13)$$

where $V_{AJ} = B_J/\sqrt{4\pi m_H n_J}$ is the Alfvén velocity in the jet. If we assume the conservation of magnetic flux in the jet, B_J in the jet is scaled as:

$$B_J = \phi B_D (b/10R_g)^{-2} = \phi B_D (D/3R_g)^{-1}, \quad (14)$$

where the plasma density n_J in the jet is calculated through the kinetic luminosity L_J of

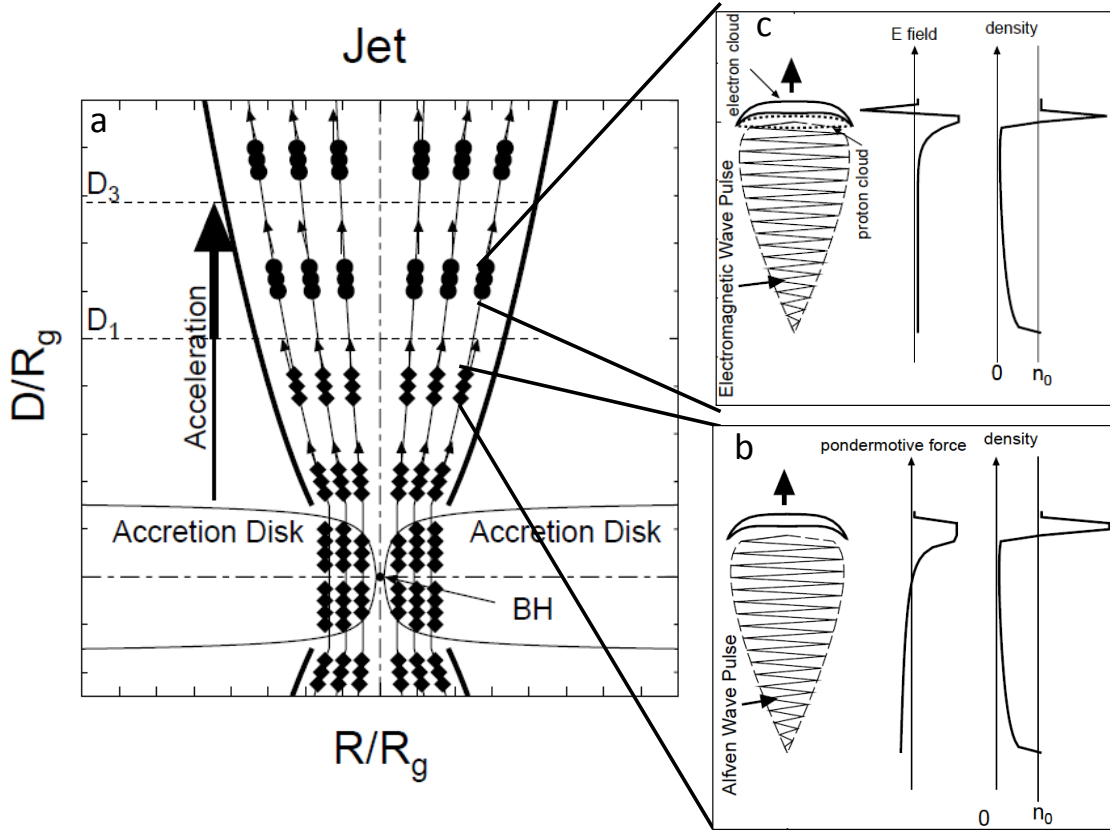


Fig. 2.— a) Schematic cross section of an disk/jet system around an accreting black hole (BH). Alfven waves (diamonds) are excited in the accretion disk and propagates along the magnetic field (thin solid curves) in the relativistic jet (thick solid curves). b) In the ponderomotive region ($\omega'_c > \omega'_p > \omega_A$), the ponderomotive force of the intense Alfven wave pulse produces a bubble and accelerate particles. c) The Alfven waves turn into electromagnetic waves (circles) as ω_A approaches and exceeds ω'_p and excites wakefields whose electric fields accelerate charged particles longitudinally along the jet. We anticipate that in the extremely large a , the domain of wakefield acceleration is dwarfed by that of ponderomotive acceleration in the 1D situation. In 2-3D, wakefield acceleration takes a greater role than in 1D.

the jet,

$$L_J = n_J m_H c^3 \Gamma^2 \pi b^2 = \xi L_{\text{tot}}. \quad (15)$$

$$n_J = 2.6 \times 10^3 (\dot{m}/0.1) (m/10^8)^{-1} (\xi/10^{-2}) (\Gamma/20)^{-2} (D/3R_g)^{-1} \text{ cm}^{-3} \quad (16)$$

The effective plasma frequency ω'_p is calculated as

$$\omega'_p = (4\pi n_J e^2 / m_e \gamma \Gamma^3)^{1/2} \quad (17)$$

$$= 2.1 \times 10^{-1} (\Gamma/20)^{-5/2} (\xi/10^{-2})^{1/2} (\dot{m}/0.1)^{-1/4} (m/10^8)^{-3/4} (D/3R_g)^{-1/4} \text{ Hz}, \quad (18)$$

On the other hand, the effective cyclotron frequency ω'_c is derived as

$$\omega'_c = e B_J / m_e c \gamma = 2.3 \times 10^0 (\phi/2.0) (\dot{m}/0.1)^{-3/2} (m/10^8)^{-1} (D/3R_g)^{-1/2} \text{ Hz}, \quad (19)$$

As an Alfvén wave pulse propagates along the jet, the density and magnetic fields decrease, and accordingly the ratios ω'_p/ω_A and ω'_c/ω_A plummet, as seen in figure 3 (for the case of $\dot{m} = 0.1$, $m = 10^8$, $\gamma = 20$, and $\xi = 10^{-2}$). As ω'_p approaches ω_A , the whistler branch of the Alfvén pulse turns into the electromagnetic wave (Chang et al. (2009)) and start to excite wakefields. The distance D_1 at which $\omega'_p = \omega_A$ is calculated as:

$$D_1/3R_g = 1.7 \times 10^3 (\Gamma/20)^{-10} (\xi/10^2)^2 (\dot{m}/0.1)^3 (m/10^8). \quad (20)$$

On the other hand, the distance D_2 at which $\omega'_c = \omega_A$ is calculated as:

$$D_2/3R_g = 5.1 \times 10^3 (\dot{m}/0.1)^{-1} (\phi/2.0)^2, \quad (21)$$

independent to \dot{m} nor m . As d increases and ω'_c approaches ω_A . In spite of the cyclotron resonance at ω'_c , most of the wave energy is likely to tunnel from the whistler branch to the upper branch beyond the right-hand cut-off frequency

$$\omega_c^{\text{rh}} = [(\omega'_c)^2 + 4(\omega'_p)^2]^{1/2} + \omega'_c / 2, \quad (22)$$

which is located above the cyclotron resonance ω'_c in the case of the cold and linear limit [Ichimaru (1973)]. In addition to the linear evanescent tunneling, the nonlinear nature of the EM waves (Ashour-Abdalla et al. (1981); $a \gg 1$) results in the resonance broadening and the nonlinear tunneling.

3. Highest energy cosmic rays

The phase velocity of Alfvén wave in the jet is close to the light velocity because of the small n_J compared to n_{SS} . In such a case, the particles are accelerated by the ponderomotive force parallel to the direction of the propagation of the wave. The maximum energy W_{PM} in the observer's frame of the particles gained in the region is calculated as:

$$W_{\max} = z \int_0^{D_3} F_{\text{pm}} dD \quad (23)$$

$$= 4.6 \times 10^{19} z (\Gamma/20) (\dot{m}/0.1)^{1/2} (m/10^8)^{1/2} (D_3/3R_g)^{1/2} \text{ eV} \quad (24)$$

$$= 2.9 \times 10^{22} z (\Gamma/20) (\dot{m}/0.1)^{4/3} (m/10^8)^{2/3} \text{ eV}, \quad (25)$$

(Ashour-Abdalla et al. (1981)) where

$$F_{\text{pm}} = \Gamma m_e c a \omega_A \quad (26)$$

is the ponderomotive force of the wave. The acceleration length is assumed to be:

$$Z_{\text{acc}} = c a / \omega_A. \quad (27)$$

This is consistent with Ashour-Abdalla et al. (1981). Further, Berezhiani & Murusidze (1990) obtained an exact nonlinear longitudinal plasma wave solution excited by a relativistic laser pulse, neglecting the quiver motion of protons. They found that the acceleration length is increased by a factor of a . This nature of acceleration lengthening

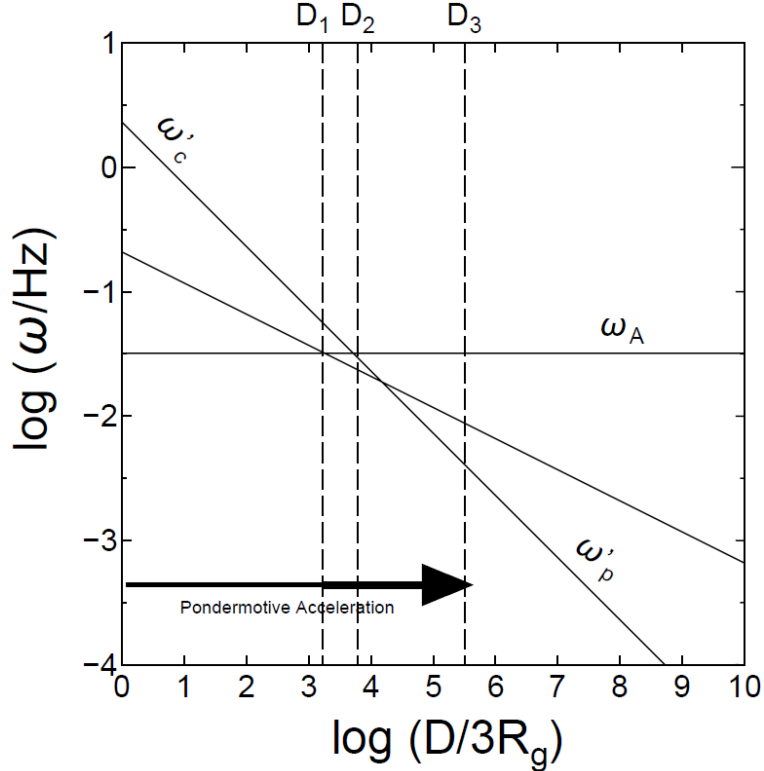


Fig. 3.— Plasma frequency ω'_p and cyclotron frequency ω'_c are plotted against distance D along the jet for the case of $\dot{m} = 0.1$, $\xi = 10^{-2}$, $\Gamma = 20$, and $m = 10^8$. The pulse of Alfvén wave with a frequency ω_A is excited in the accretion disk ($D/R_g = 1$), propagating along the jet. Both ω'_p and ω'_c decrease as D increases. The Alfvén wave (whistler branch) turns itself into electromagnetic pulse around where $\omega'_p = \omega_A$ and drive wakefields to accelerate charged particles along the jet. Further mode-conversions are possible beyond $\omega_A > \omega'_c$. In this figure, we show the dominance of the pondermotive acceleration in the extreme regime of $a \gg 1$ in 1-D.

can be expected to remain even in the case that proton quiver motion is not negligible, i.e., $a > 10^3$. They also found the plasma density is significantly reduced in the relativistic laser pulse because the plasma is evacuated by the strong ponderomotive force. Equation 25 holds as far as Z_{acc} is greater than D . The distance D_3 is where the acceleration finishes, defined by the equation

$$D_3 = Z_{\text{pd}} = ac/\omega_A. \quad (28)$$

We find that particles arrive at D_1 before D_3 , in other words:

$$D_3/3R_g = 3.9 \times 10^5 (\dot{m}/0.1)^{5/3} (m/10^8)^{1/3} > D_1/3R_g. \quad (29)$$

The energy spectrum of the accelerated charged particles has the power-law with the index of -2 due to the multiple dephasing occurrences when particles ride on and off different peaks of the ponderomotive or wakefield hills when the waves contain multiple frequencies (but with again the same phase velocity $\sim c$; Chen et al. (2002)), i.e., $f(W) = A(W/W_{\min})^{-2}$. As noted earlier, when the driving Alfvén waves and their driven wakefields hold a broad band of frequencies, their phase velocities and group velocities, respectively, are again close to the speed of light, providing the basis for the robust accelerating structure. When wakefields have two or three dimensional features, the dephasing is prompted, leading to higher index of the spectrum (less than -2). Let κ be the energy conversion efficiency of the acceleration (including the mode convergence efficiency mentioned earlier), then $\kappa E_B = AW_{\min}^2 \ln(W_{\max}/W_{\min})$, i.e.

$$A = 1.6 \times 10^{33} \kappa \dot{m} m^2 [W_{\min}^2 \ln(W_{\max}/W_{\min})]^{-1}. \quad (30)$$

The recurrence rate ν_A of the Alfvén pulse burst is evaluated as:

$$\nu_A = \eta V_{\text{AD}}/Z_D = 1.0 \times 10^2 \eta m^{-1} \text{ Hz}, \quad (31)$$

where η is the episode -dependent on the order of unity. This is consistent with the 3-dimensional simulations conducted by O'Neill et al. (2011). They found magnetic

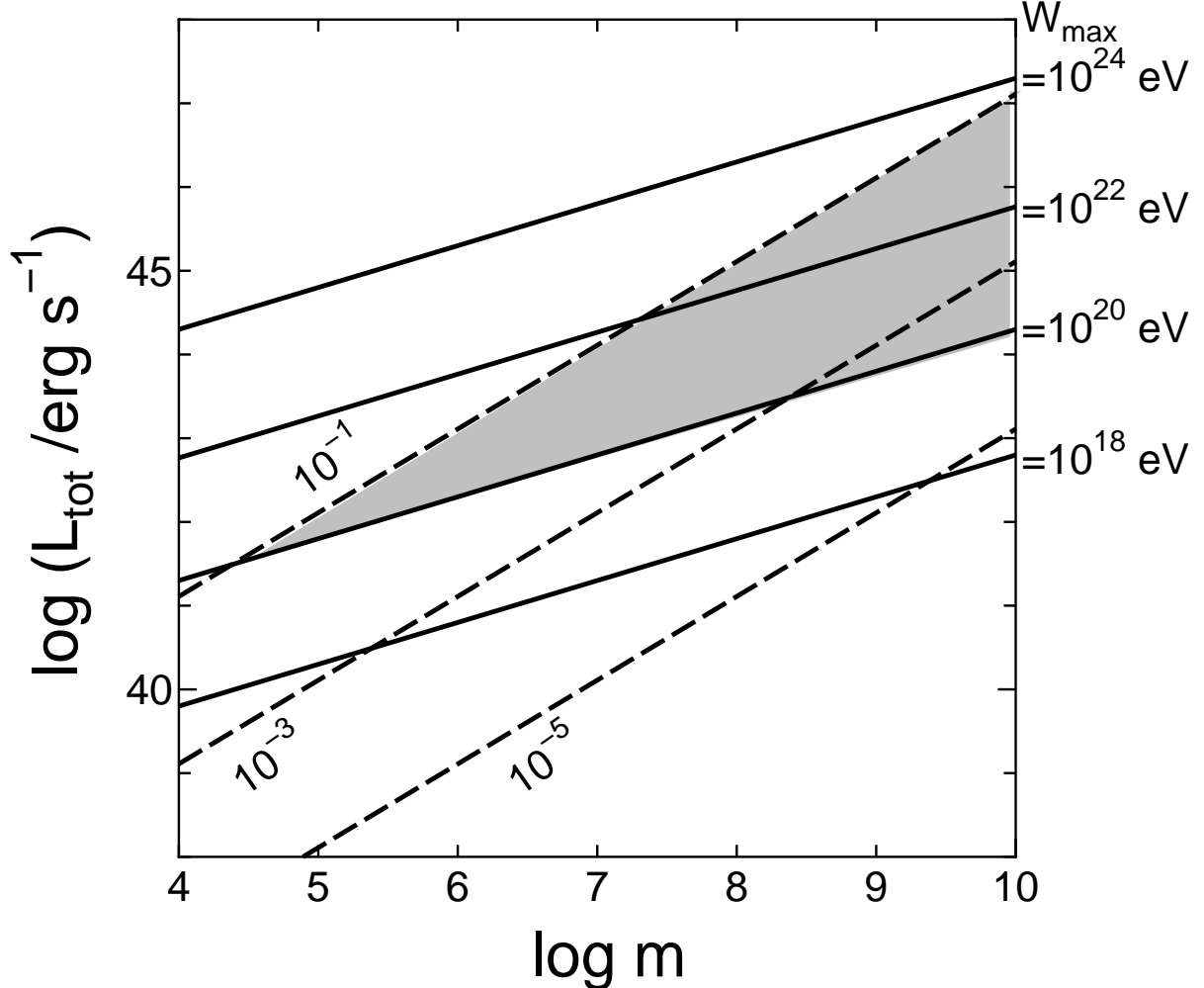


Fig. 4.— The total luminosities of accreting blackholes are plotted against the blackhole mass (in the unit of solar mass) for various maximum attainable energy W_{\max} (solid lines) for the case of $\Gamma = 20$ and $\xi = 10^{-2}$. Dashed lines represent the lines for $\dot{m} = 10^{-5}, 10^{-3}$, and 10^{-1} , respectively. The grey triangle represents the parameter sets which allow the acceleration of UHECRs ($\geq 10^{20}$ eV). We may set the upper limit of \dot{m} to be around 0.1 for the ponderomotive/wakefield acceleration may work, since the accretion disk becomes radiation dominant, as \dot{m} approaches unity, so that an Alfvén wave pulse becomes weaker than estimated in the present paper.

fluctuations, called Long Period Quasi Periodic Oscillations (LPQPO) with the period 10-20 times the Kepler rotation period. The luminosity L_{UHECR} of ultra-high energy cosmic rays is:

$$L_{\text{UHECR}} \sim \kappa \zeta E_B \nu_A = 1.6 \times 10^{33} (\kappa \zeta / 0.01) \eta \dot{m} m \text{ erg s}^{-1}, \quad (32)$$

where $\zeta = \ln(W_{\text{max}}/10^{20} \text{ eV})/\ln(W_{\text{max}}/W_{\text{min}})$.

The wakefields in the jets accelerate both ions and electrons and therefore the AGN jet is likely to be strong gamma-ray sources as well. Although the radiation loss of protons and nuclei is negligible as far as they are accelerated parallel to the magnetic field (Jackson (1963)), that of electrons is likely to be significant, when electrons encounter magnetic fluctuations. The gamma-ray luminosity is, therefore, found to be as:

$$L_{\gamma} \sim \kappa E_B \nu_A = 1.6 \times 10^{34} (\kappa / 0.1) \eta \dot{m} m \text{ erg s}^{-1}. \quad (33)$$

We summarize the major features of ponderomotive/wakefield acceleration in an accreting supermassive blackhole in Table 1.

4. Astrophysical implications and blazar characteristics

Radio galaxies belong to one category of AGN, which has radio lobes connected to the nucleus by relativistic jets. Their central engines are accreting supermassive ($m = 10^6 - 10^{10}$) blackholes. Urry & Padova (1991) pointed out that they are parent (or misaligned) populations of blazars, which show rapid time variations in many observational bands across radio to gamma rays (10 GeV) with distinct optical and radio polarizations because of their relativistic jet pointing almost toward us. The recent observation by the Fermi satellite reveals that many blazars emit strong gamma-rays in the GeV energy range (Hartman et al. (1999); Ackermann et al. (2011)).

We find that radio galaxies are most likely to be sources of UHECRs and their features fit well with the wakefield theory of acceleration. First, according to Ajello et al. (2012) and Broderick (2012), the local gamma-ray luminosity density of blazars is estimated as $10^{37-38} \text{ erg s}^{-1} (\text{Mpc})^{-3}$, taking into account the beaming effect of the relativistic jet. Assuming $L_{\text{UHECR}}/L_{\gamma} \sim \zeta \sim 0.1$ (see table 1), our theoretical estimate of UHECR particle flux, averaged over the sky, becomes:

$$\overline{\Phi_{\text{UHECR}}} = 7.6 \times 10^{-2} l_{\gamma 37} (\zeta/0.1) (\tau_8/1.5) \text{ particles}/(100 \text{ km}^2 \text{ yr sr}). \quad (34)$$

Equation 34 is consistent with observed flux of UHECR. Here, $l_{\gamma 37}$ is the local gamma-ray luminosity density of blazars in the unit of $10^{37} \text{ erg s}^{-1} (\text{Mpc})^{-3}$ and τ_8 is the life time of UHECR particles (in the unit of 10^8 yr), which is determined by GZK process: Greisen (1966) and Zatsepin & Kuzmin (1966) predicted that cosmic-ray spectrum has a theoretical upper limit around $5 \times 10^{19} \text{ eV}$, because of the opening of the channel to produce Δ^+ particles, which decay into pions (π^0 and π^\pm) and further into photons, electrons, protons, neutrons, and neutrinos. The flux of the cosmogenic neutrinos, produced by the GZK process, is as high as

$$\overline{\Phi_{UHE\nu}} = 5.4 \times 10^{-1} l_{\gamma 37} (\zeta/0.1) (\tau/100) \text{ particles}/(100 \text{ km}^2 \text{ yr sr}), \quad (35)$$

Table 1: Major features of wakefield acceleration in an accreting supermassive blackhole.

	values	units
$2\pi/\omega_A$	$2.0 \times 10^2 (\dot{m}/0.1)(m/10^8)$	s
$1/\nu_A$	$1.0 \times 10^6 \eta^{-1} (m/10^8)$	s
D_3/c	$1.2 \times 10^9 (\dot{m}/0.1)^{5/3} (m/10^8)^{4/3}$	s
W_{\max}	$2.9 \times 10^{22} z (\Gamma/20) (\dot{m}/0.1)^{4/3} (m/10^8)^{2/3}$	eV
L_{tot}	$1.2 \times 10^{45} (\dot{m}/0.1)(m/10^8)$	erg s^{-1}
L_A	$1.2 \times 10^{42} \eta (\dot{m}/0.1)(m/10^8)$	erg s^{-1}
L_γ	$1.2 \times 10^{41} (\eta \kappa/0.1)(\dot{m}/0.1)(m/10^8)$	erg s^{-1}
L_{UHECR}	$1.2 \times 10^{40} (\eta \kappa \zeta/10^{-2})(\dot{m}/0.1)(m/10^8)$	erg s^{-1}
$L_{\text{UHECR}}/L_{\text{tot}}$	$1.0 \times 10^{-5} (\eta \kappa \zeta/10^{-2})$	-
$L_{\text{UHECR}}/L_\gamma$	$1.0 \times 10^{-1} (\zeta/0.1)$	-

$\xi = L_J/L_{\text{tot}}$, $\eta = \nu_A Z_D/V_A$, $\kappa = E_{\text{CR}}/E_A$, and $\zeta = \ln(W_{\max}/(10^{20} \text{eV}))/\ln(W_{\max}/W_{\min})$.

assuming the conversion efficiency of UHECR to UHE ν to be 10%. This is consistent with the previous works for the case of $W_{\max} = 10^{21.5}$ (e.g. Kotera et al. (2010)). The recently observed PeV neutrinos with Ice Cube experiment (Arlen et al. (2013)) is also consistent if we assume the power law spectrum of the index of -2.2 in the energy region from PeV to ZeV (Barwick et al. (2013)). A next generation space borne detector of UHECR, like JEM-EUSO, which can achieve an integrated exposure of $10^6 \text{ km}^2 \text{ str yr}$ (Takahashi et al. (2008); Kajino et al. (2009); Gorodetzky (2011)), may detect this level of UHE ν flux (Santangelo et al. (2010)).

Second, blazars are also known for being highly variable at all wavelengths and all time scales. In the most extreme cases, the timescales of gamma-ray variability can be as short as a few minutes at very high energies ($\sim 100 \text{ GeV}$; VHE). Such variability has been detected in several BL Lacertae objects (Arlen et al. (2013); Gaido et al. (1996); Albert et al. (2007); Aharonian et al. (2007); Aleksic et al. (2011); Saito et al. (2013)). On the other hand, our wakefield acceleration mechanism predicts the rapid time variability with all the time scales from the Alfvén frequency ($2\pi/\omega_A \sim 100 \text{ s}$), through the repetition period of the pulses ($1/\nu_A \sim \text{days}$), and to the propagation time in the jet ($D_2/c, 1 \sim 10^2 \text{ years}$). This time variability is both for ion acceleration variability for UHECRs as well as electron variability as observed in gamma rays (electron energies are limited by the radiation energy loss by PeV (Deng et al. (2012))). The finer structure of time variability is anticipated from our mechanism, as the magnetic structure may contain finer structure of braiding within the above quoted Alfvén pulse. These observed blazer variabilities are the natural consequences deeply embedded in our model. Further, the coincidence of the pronounced luminosity peak and the reduced spectrum index observed Fermi satellite (Abdo et al. (2010)) of BL Lacs has so far no known explanation offered but it is consistent with our theory (Abazajian et al. (2013)).

Third, the multiple epoch observation of VLBA provides a strong evidence that gamma-ray emission comes from parsec scale jet (Lister et al. (2009); Marscher et al. (2010); Lyutikov & Lister (2011)). Since the life time of high energy electrons is much shorter than the propagation time, they must be locally accelerated. This is consistent with the picture of the wakefield acceleration, since a swarm of the electrons is accelerated locally in the wakefields propagating in the jets. They are likely to emit a highly variable and polarized gamma-rays due to their high gamma-factor.

Our calculation shows the UHECR flux of a gamma-ray emitting galaxy as:

$$\Phi_{\text{UHECR}} = 3.5 \times 10^{-3} (\zeta/0.1) (\Phi_{\gamma}/10^{-10} \text{ photons cm}^{-2} \text{ s}^{-1}) (\overline{E_{\gamma}}/1 \text{ GeV}) \text{ particles}/(100 \text{ km}^2 \text{ yr})^{-1}, \quad (36)$$

if the radiation pattern of UHECRs is the same as that of gamma-rays. Here, Φ_{γ} is the gamma-ray flux and $\overline{E_{\gamma}}$ is the average gamma-ray energy. We found nine gamma-ray emitting AGNs (Ackermann et al. (2011)) within the GZK horizon (≤ 70 Mpc; Table 2). The spectral indices are in the range of $-2 \sim -2.8$, which are consistent with our theory. Figure 5 shows the distribution of these gamma-ray emitting AGNs in the sky. This value is large enough to be identified as an individual source by a cluster of events with JEM-EUSO as well (Takahashi et al. (2008); Kajino et al. (2009); Gorodetzky (2011)).

5. Conclusions

We have introduced the wakefield acceleration mechanism arising from the Alfvénic pulse incurred by an accretion disk around an supermassive blackhole, the central engine of AGN. This provides a natural account for UHECRs, and also the accompanying gamma-rays and their related observational characteristics, such as their luminosities, time variations, and structures. The severe physical constraints in the extreme ZeV energies by the Fermi acceleration have been lifted by the present mechanism. We have identified a number

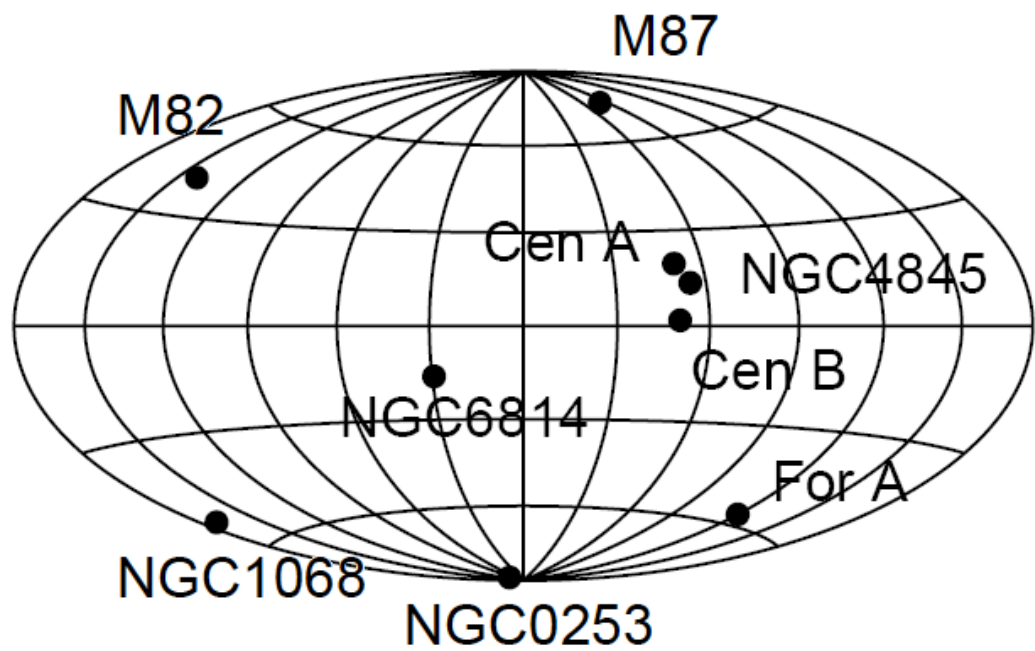


Fig. 5.— Distribution of the nine gamma-ray emitting AGNs (Ackermann et al. (2011)) in the sky

Table 2: Nearby gamma-ray emitting AGNs detected by Fermi satellite (Ackermann et al. (2011))

Counterpart	LII	BII	Redshift	Flux (1GeV-100GeV)	Spectral Index
				$10^{-10} \text{ erg cm}^{-2}$	
NGC 0253	97.39	-87.97	0.001	6.2 ± 1.2	2.313
NGC 1068	172.10	-51.04	0.00419	5.1 ± 1.1	2.146
For A	240.15	-56.70	0.005	5.3 ± 1.2	2.158
M82	141.41	40.56	0.001236	10.2 ± 1.3	2.280
M87	283.78	74.48	0.0036	17.3 ± 1.8	2.174
Cen A Core	309.51	19.41	0.00183	30.3 ± 2.4	2.763
NGC 4945	305.27	13.33	0.002	7.5 ± 1.7	2.103
Cen B	209.72	1.72	0.012916	18.6 ± 3.5	2.325
NGC 6814	29.35	-16.02	0.0052	6.8 ± 1.6	2.544

of areas of future research that needs further studies, including the bubble dynamics of super-intense Alfvén pulses in 1-3 dimensions. We have already seen a number of emerging astrophysical phenomena that are not easy to explained by existing theories, but are in line with natural consequences of the present acceleration mechanism.

We would like to dedicated this paper to the late Professor Yoshiyuki Takahashi, whose encouragement on this work has been crucial. We appreciate the discussion with Profs. K. Abazajian, S.W. Barwick, S. Nagataki, A. Mizuta, and G. Yodh.

REFERENCES

Aartsen, M.G. et al. to be published in PRL

Abazajian, K. Tajima, T., and Ebisuzaki, T. 2013, to be published.

Abdo A.A. et al. 2010, ApJ, 710, 1271

Ajello, M. et al. 2012, ApJ, 751, 108

Ackermann, M., Ajello, M., Allafort, A., et al. 2011, ApJ, 743, 171

Aharonian, F., Akhperjanian, A. G., Bazer-Bachi, A. R., et al. 2007, ApJ, 664, L71

Albert, J., Aliu, E., Anderhub, H., et al. 2007, ApJ, 666, L17

Aleksic, J., Antonelli, L. A., Antoranz, P., et al. 2011, ApJ, 730, 8

Arlen, T. et al. 2013, ApJ, 762, 92

Asada, K. and Nakamura, M. 2012, ApJ, 745, L28

Ashour-Abdalla, M., Lebouf, J.N., Tajima, T., Dawson, J. M., and Kennel, C. F., 1981, Phys. Rev. A. 23, 1906

Barwick, S., Abazjian, K., Tajima, T., and Ebisuzaki, T. 2013, to be published.

Berezhiani V.I. and Murusidze, I.G. 1990, Physics Letters, A. 148, 338-340.

Blandford, R. D. and Znajek, R. L. 1977, MNRAS, 179, 433

Broderick, A.E. 2012, ApJ, 752, 22

Bulanov, S.V. Esirkepov, T., Kando. M.Pirozhkov, N. 2013, Phys. -Uspekhi, 56, 429.

Chang, F.Y. et al. 2009, Phys. Rev. Lett. 102, 111101

Chen, P.C., Tajima, T., and Takahashi, Y. 2002, Phys. Rev. Lett. 89, 161101

Deng, A. et al., 2012, Phys. Rev. STAB 15, 081303

Esarey, E. and Piloff, M. 1995, 2, 1432

Esarey, E., Schroeder, C.B., and Leemans, W.P. 2009, Rev. Mod. Phys., 81, 1229

Fermi, E., 1954 ApJ, 119, 1

Gaidos, J. A., Akerlof, C. W., Biller, S., et al. 1996 Nature, 383, 319

Gorodetzky P. et al. 2011, Nucl. Inst. & Meth. in Phys. Res. Sect. A, 626, S40

Greisen, K., Phys. Rev. Let. 1966, 16, 748

Hartman, R. C., Bertsch, D. L., Bloom, S. D., et al. 1999, ApJS, 123, 79

Hillas, A. M., 1984, Ann. Rev. Astron. Astrophys., 22, 425

Ichimaru, S., 1973, Basic Principle of Plasma Physics, Benjamin, Reading, p.89

Jackson, J.D. 1963, Classical Electrodynamics, John Wiley and Son.

Kajino, F. et al. 2009, Nuclear Instruments & Methods, 1, 422

Kotera, K., Allard, D., and Olinto, A., 2010, J. of Cosmology & Astroparticle Physics, 10, 013

Kotera, K. and Olinto, A. 2011, Ann. Rev. Astron. Astrophys., 49, 119

Leemans, W., Chou, W., and Uesaka, M., 2011, in ICFA Beam Dynamics Newsletters, 56, 10

Lister, M. L., et al. 2009, AJ, 137, 3718

Lyutikov, M. and Lister, M. 2010, *ApJ*, 722, 197

Marscher, A. P., & Jorstad, S. G. 2010, *ApJ*, 710, L126

Matsumoto, R. and Tajima, T., 1995, *ApJ*, 445, 767

Mima, K., Horton W., Tajima, T., and Hasegawa, A., in *Nonlinear Dynamics and Particle Acceleration*, eds. Y. Ichikawa and T. Tajima (AIP, NY, 1991), p27

Mourou, G.A., Tajima, T., and Bulanov, S., 2006, *Rev. Mod Phys.* 78, 309-371.

Nakar, E., 2007, *Phys. Rep.* 442, 166

O'Neill, S.M., et al. 2011, *ApJ*, 736, 107

Saito, S. et al. 2013, *ApJ*, 766, L11.

Santangelo, A. 2010, *Progress in Particle and Nuclear Physics*, 64, 366

Shakura, N.I. and Sunyaev, R.A. 1973, *A&A*, 24, 337

Shibata, K., Tajima, T., and Matsumoto, R., 1990, *ApJ*, 350, 295

Tajima, T. 2010, *Proc. Jpn. Acad. Sci.*, B86, 147.

Tajima, T. and Dawson, J. M., *Phys. Rev. Lett.* 1979, 43, 267

Takahashi, Y., Tajima, T., and Hillman, L. 2000, in *High Field Science*, eds. T. Tajima, K. Mima, and H. Baldis, Klewer, p. 171

Takahashi, Y. et al. 2008, *New J. of Phys.*, 11, 065009

Takahara, F. *Prog. Theor. Phys.* 1990, 83, 1071

Urry, C.M., & Padovani, P. 1991, *ApJ*, 371, 60

Zatsepin, G.T. and Kuzmin, V.A. 1966, JETP Lett. 4, 78